A Study of SSM/I-Derived Columnar Water Vapor over the Global Oceans

DARREN L. JACKSON

Cooperative Institute for Research in Environmental Sciences (CIRES), University of Colorado/NOAA, Boulder, Colorado

GRAEME L. STEPHENS

Department of Atmospheric Science, Colorado State University, Fort Collins, Colorado

(Manuscript received 16 April 1994, in final form 25 February 1995)

ABSTRACT

Four years of columnar water vapor (CWV) data from July 1987 through June 1991 derived from a satellite-based physical retrieval method are analyzed using microwave observations from the Special Sensor Microwave/Imager. This retrieval along with three statistically based retrievals were compared to radiosonde data compiled for the GEWEX Water Vapor Project. It is shown that the root-mean-square (rms) difference (R) between the radiosonde data and these satellite retrievals ranges from 4.66 kg m^{-2} to 5.08 kg m^{-2}. The rms difference was found to have a seasonal variability of up to 1.0 kg m^{-2} with the highest R in JJA. It was also found to significantly depend on the specified time and spatial coincidence of the satellite pixels with the radiosonde observation. The rms difference decreased by about 0.65 kg m^{-2} when the time constraint was reduced from 2 h to 0.5 h, but R *increased* by about 0.3 kg m^{-2} when the spatial coincidence was reduced from 50 to 20 km. The relationship between 4 yr of CWV and SST data was found to vary significantly with season and hemisphere. The correlation between 4 yr of monthly mean, globally averaged SST and CWV was approximately 0.95 for the hemispheric means and 0.65 for the global means. The 4-yr correlation of SST and CWV was found to be strongest in the subtropical regions and weakest in several tropical regions.

1. Introduction

Observing the temporal and spatial variations of water vapor over the globe is considered essential for addressing fundamental issues dealing with the earth's climate and is a major goal of the GEWEX Water Vapor Project (GVaP; Starr and Melfi 1990). The transport and phase change of water vapor shape the diabatic processes that drive the general circulation and affect the radiative transfer within the atmosphere. Diagnosing the distribution of water vapor in the atmosphere using remote sensing methods is thus vital for studying these aspects of the earth's climate system especially in regions that are not accessible to conventional radiosonde observations.

Through improved remote sensing methods and radiometric technology, the ability to retrieve water vapor over the globe has improved substantially over the past few decades. Pioneering studies by Benton and Estoque (1954) and Starr et al. (1969) first began the investigation of the global distribution and transport of water vapor using a global network of radiosondes. Their work laid the foundation for much of the climate research investigating water vapor's role in climate. However, a problem inherent to these early studies is the bias these data contained due to few measurements over the oceans. The development of satellite radiometers over the past two decades has opened the passage for remote sensing techniques that can provide much higher horizontal resolution of CWV over the entire globe.

Two primary regions of the electromagnetic spectrum used to retrieve water vapor information from satellites are in the infrared (IR) and microwave. Water vapor retrievals in the IR have been accomplished from the GOES VAS channels (e.g., Smith 1983) and from the High Resolution Infrared Radiation Sounder (HIRS/2) channels (Hillger and Vonder Haar 1981). The well-known TIROS Operational Vertical Sounder (TOVS) incorporates data from the HIRS/2 instrument into an algorithm used to derive the TOVS global water vapor datasets. These datasets provide coarse vertical resolution and complete global coverage of water vapor (Smith et al. 1979). However, the limitation of the measurements from IR instruments is their inability to retrieve water vapor in cloudy regions. Passive microwave retrieval methods have been recognized as a complement to the IR methods because the microwave retrievals can be performed in cloudy regions as well. This advantage is particularly important for understanding the relationship between clouds and water vapor (Gaffen and Elliot 1993; Stephens et al. 1994).

Corresponding author address: Mr. Darren L. Jackson, CIRES, University of Colorado, Campus Box 449, Boulder, CO 80309-0449.

The two disadvantages of most microwave approaches lie in their inability to retrieve water vapor over land and retrieve the vertical distribution of water vapor. These disadvantages have made themselves evident in the past since all passive microwave instruments devoted to measuring water vapor have had channels near the 22-GHz water vapor absorption line and at nearby window frequencies. The 22-GHz absorption line is too weak to provide reliable vertical profiles of water vapor. Furthermore, since the weighting functions at these frequencies generally reach a peak at the surface (excluding precipitating clouds), the large and highly variable emission from land surfaces, which depends on changing vegetation and soil moisture, among other factors, will have a dominant influence on the measured radiances. However, retrieving water vapor soundings from microwave measurements will be possible using new data from the SSM/T2 instrument (Leute 1993), where measurements of the absorption line at 183 GHz may be able to provide water vapor information for a few vertical layers.

Several microwave methods have been introduced to retrieve CWV, yet no comprehensive published study has assessed the differences between physical and statistical methods or the differences between these methods and radiosonde data. Jackson (1992) analyzed both physical and statistical satellite methods; however, his study was limited by comparing radiosonde data with unknown quality controls. Biases may arise in physical methods through model approximations and from constraints imposed on the physical variables, whereas biases may be introduced in statistical methods through the selection of a reference radiosonde dataset. Differences in the quality control measures used to screen out retrievals contaminated by precipitation and sea ice may also lead to differences in the CWV datasets. These problems are addressed in this paper and an intercomparison of a selection of the currently available retrieval methods are discussed.

Examining the relationship between SST and water vapor is considered important for better understanding the general circulation and hydrologic processes. Stephens (1990) used this relationship to describe large-scale dynamical features of the general circulation. Liu (1988) derived monthly mean moisture and latent heat fluxes using satellite estimates of CWV, SST, and surface wind speed. Liu et al. (1991) shows a close relationship between the surface specific humidity and CWV, which could be used to investigate evaporation rate over the oceans. Therefore, important processes can be studied given a known relationship between CWV and SST.

The primary objectives of this paper are to describe a 1-yr intercomparison of CWV derived from four satellite retrieval methods using SSM/I and radiosonde data and to describe the 4-yr relationship between CWV and SST. A 1-yr comparison of the Greenwald et al. (1995) method (hereafter referred to as the GRE method) to the statistical methods of Alishouse et al. (1990) (ALI) and Petty (1994) (PET) and the semi-statistical method of Schluessel and Emery (1990) (SCH) is performed using identical quality controls. A comparison is also made between a global radiosonde dataset designed for GVaP and these four satellite retrievals. Analysis of the interannual and seasonal variations of CWV derived from the GRE method and its relationship with Reynolds' SST (Reynolds 1988) are also described.

This paper begins in section 2 with a description of the SSM/I. Section 3 discusses the retrieval characteristics and quality controls used on the satellite data. Section 4 presents the statistical retrieval comparison and radiosonde validation, section 5 discusses the relationship between CWV and SST, and section 6 details the conclusions.

2. SSM/I data characteristics

The SSM/I instrument that provided the brightness temperature data used in this study flew on board the Defense Meteorological Satellite Program (DMSP) Block 5D-2 Spacecraft F08. The SSM/I instrument is a passive microwave radiometer that measures microwave emission from the earth's surface and its atmosphere at four different frequencies. Horizontal and vertical polarization measurements are taken at 19.35, 37.0, and 85.5 GHz, whereas the 22.235-GHz channel measures only the vertical polarization. The spatial resolution depends on frequency with the highest resolution (15 km × 13 km) at 85.5 GHz and the lowest resolution (69 km × 43 km) at 19.35 GHz. Complete global coverage except near the poles is achieved in 2 to 3 days. Conversion of the raw antenna temperatures into brightness temperatures was done using a technique provided in Wentz (1992). Precision errors in the brightness temperatures were stated in Wentz (1992) to be less than 0.1 K for a range of antenna temperatures from 176 to 270 K. Characteristics of the SSM/I and the orbital parameters of the DMSP satellite are described in Wentz (1992).

Table 1 shows the days with no SSM/I data during the 4-yr period from July 1987 to June 1991. December has the worst sampling because the instrument was turned off in December 1987 due to excessive solar heating of the instrument. It should be noted that Table 1 does not indicate the amount of missing data on days containing any good data.

3. Retrieval characteristics and quality control

Using the SSM/I brightness temperatures, the GRE method was used to retrieve CWV and integrated cloud liquid water (CLW). This method takes advantage of the water vapor characteristics at both 19 and 22 GHz and uses only the vertical (V) polarization channels to minimize sea surface roughness effects. The 22V and

TABLE 1. Number of complete days missing from the raw SSM/I data for the F08 satellite from 9 July 1987 to 31 December 1991.

	1987	1988	1989	1990	1991	Total days
January	NA	1st–12th	19th	—	—	13
February	NA	—	—	—	—	0
March	NA	—	—	—	—	0
April	NA	—	—	—	—	0
May	NA	6th–8th	—	—	—	3
June	NA	—	8th	—	20th–23rd	5
July	1st–8th	—	23rd–24th	—	NA	10
August	25th–26th	—	—	25th–26th	NA	4
September	—	23rd	—	—	NA	1
October	6th–7th	23rd	23rd	—	NA	4
November	—	—	—	—	NA	0
December	1st–31st	25th–27th	—	22nd–26th	NA	39
Total days	43	20	5	7	4	79

37V channels are used exclusively for CWV < 53.4 kg m^{-2} since this combination of frequencies produces less random scatter in the retrievals. Since the 22-GHz channel has a reduced sensitivity to changes in water vapor for extremely moist atmospheres, a weighted combination of the 22V/37V and 19V/37V retrievals is used for CWV > 53.4 kg m^{-2}. Refer to Greenwald et al. (1995) for a more complete discussion of the retrieval method.

The retrieval of 4 years (July 1987–June 1991) of monthly mean CWV and CLW was performed using the GRE method, and 1 year (1989) of monthly mean CWV was made using the methods of ALI, PET, and SCH. One aspect of the quality control procedure involved eliminating SSM/I data that had been mislocated due to erroneous time tags (Wentz 1992). An important quality control measure was to remove retrievals mostly contaminated by precipitation, which was determined from retrievals of CLW exceeding 0.4 kg m^{-2} [see Greenwald et al. (1995) for details]. All land areas were removed using a 0.5° land mask, and the removal of pixels within 0.5° of a land-masked grid box was performed to eliminate any unwanted sidelobe contamination from the lowest-frequency channels. Sea ice contamination was also removed from these data using the simple version of the AES/YORK algorithm that was developed for the SSM/I Cal/Val effort (Hollinger et al. 1991). The final processing step was to bin the pixel data into a 1° resolution grid.

4. Radiosonde validation and algorithm comparison

The purpose of this section is to demonstrate how the daily and seasonal CWV mean and variance fields predicted by the GRE method compare with other retrievals and to assess the relative accuracy of these retrievals with ground observations using identical quality control procedures for precipitation, sea ice, and land contamination. Quality control plays an important role in comparing different retrieval methods, and different quality control procedures, particularly with precipitation contamination, can significantly affect both the daily and monthly averaged CWV. Therefore, if any pixel was found to contain significant precipitation (i.e., for CLW > 0.4 kg m^{-2}), then the entire radiosonde observation and its corresponding satellite observations were removed from data. Also, it is generally difficult to assess the accuracy of a satellite-based retrieval method since ground-based measurements almost never coincide in space and time with satellite measurements. Even for perfect coincidence, inherent errors and biases introduced by different sampling and instrumentation make the task of validation most difficult. All space and radiosonde data comparisons in this study restrict the time coincidence to at most 2 h and the spatial coincidence to at most 50 km in order to best compare these two different measurements.

The current water vapor retrieval methods can be categorized into three types: physical, semistatistical, and statistical methods. The physical methods are based on an inverted form of the radiative transfer equation and use the observed brightness temperatures in this inversion to solve for the CWV. Examples of physical methods are Wentz (1983), Tjemkes et al. (1991), and Greenwald et al. (1995). Schluessel and Emery (1990) and Chang and Wilheit (1979) are examples of semistatistical methods that use regression formulas to relate the brightness temperatures at the SSM/I frequencies to CWV. They establish this relationship using a radiative transfer model to predict brightness temperatures at the SSM/I frequencies based on a set of atmospheric temperature and moisture profiles which are considered representative of the global climate. The statistical methods of Petty (1994) and Alishouse et al. (1990) use nonlinear regression formulas to predict the CWV by relating brightness temperatures at several SSM/I channels to the CWV derived from the soundings of a select set of radiosonde data.

a. Radiosonde data

A global radiosonde comparison is presented in this study in order to remove regional biases from the com-

parison. Here we use the water vapor dataset prepared for GVaP by Dr. W. Elliot and colleagues. This dataset originated from the Global Telecommunication System where radiosonde observations are used to initialize forecast models and synoptic weather charts. These data are archived in their raw form at National Center for Atmospheric Research and were processed by Dr. Elliot and colleagues. The following discussion summarizes the document obtained with these data (Ross 1994, personal communication).

The water vapor dataset consists of integrated water vapor through five layers of the atmosphere: surface–850 mb, 850–700 mb, 700–500 mb, 500–400 mb, and 400–300 mb. Quality control measures included eliminating observations with any missing temperature, dewpoints, or pressure values for levels below or including 700 mb. Reasonable value checks were also made to these parameters. Temperature observations were tested against a zonal mean upper-air climatology from Oort (1983), and values were rejected if outside a liberal range from that mean. Furthermore, monthly means and standard deviations of the temperature at each level were calculated for each station and values outside of four standard deviations from the monthly mean were removed. If a failure occurred above 700 mb, the water vapor values at those levels were removed but the sounding below 700 mb was retained.

The quality control measures used in their processing did not address the bias problem introduced by instrumentation. Radiosonde instrumentation differs between countries and changes from technological advances over time (Gaffen 1993). In particular, humidity sensor types vary widely, thus causing significant biases in the humidity measurements. Biases in RH are also introduced because the lag time in instrument response creates a tendency for measurements to be biased too moist. While improvements have been made in recent years in reducing this lag time, there are still several countries using outdated humidity sensors. For example, it was found that two stations off the southwest coast of India (Minicoy and Amimu) had large differences with all satellite retrievals resulting in rms differences exceeding 20 kg m^{-2}. The lithium chloride humidity sensors still used in Indian radiosondes are known to be unreliable (Nash and Schmidlin 1987); therefore, all Indian stations were removed from the analysis.

Another limitation of these radiosonde data is that the spatial sampling is not homogeneous. Coverage is greater in the Northern Hemisphere and almost all observations are conducted over large landmasses. Therefore, finding matches between radiosonde observations over the ocean and SSM/I observations is quite sparse. There were 466 375 observations globally in the 1989 radiosonde dataset, but only 8.2% of those observations could be collocated with satellite observations. Large gaps in the data can be found in the Southern Hemispheric oceans where few islands or shipping lanes exist.

CWV was calculated from the radiosonde data in the following manner (Ross 1994, personal communication). Given the relative humidity (RH) from the data, the vapor pressure (e) can be calculated using

$$\mathrm{RH}(\%) = \left(\frac{e}{e_s}\right)100, \tag{1}$$

where the saturation vapor pressure, e_s, was found using the method presented in Buck (1981). That method determines e_s by using

$$e_s(T) = 6.1121 \exp\left[\frac{\left(18.729 - \dfrac{T}{227.3}\right)T}{T + 257.87}\right] f, \tag{2}$$

where

$$f = 1.0007 + 3.46 \times 10^{-6} p, \tag{3}$$

where T is temperature in Celsius, and p is pressure in mb. Here f is used to compensate between pure water vapor and moist air. Using the vapor pressure, e, the specific humidity is determined using

$$q = \frac{0.622e}{p - 0.379e}, \tag{4}$$

where q is units of kg kg^{-1}. The CWV can be calculated between two pressure levels using

$$\mathrm{CWV} = \frac{0.01}{g}\int_{p_1}^{p_2} q\,dp = \left(\frac{1}{g}\right)\left(\frac{q_1 + q_2}{2}\right)(p_1 - p_2), \tag{5}$$

where g is the acceleration due to gravity in m s^{-2} and CWV is expressed in units of kg m^{-2}. The factor 0.01 is used to change pressure units from mb to Pascals. In calculating CWV, the distribution of q is assumed to be linear between consecutive levels in the radiosonde data.

b. Radiosonde–satellite CWV comparison

A radiosonde comparison for the year of 1989 was performed using four satellite retrievals. The following discussion will describe differences between satellite and radiosonde CWV as biases. It should be noted that these are *relative* biases and that the radiosonde data contain biases themselves. Most notably the measurements from radiosondes above 500 mb are considered unreliable and are generally biased too moist (see section 4a).

The radiosonde locations used for this year are shown in Fig. 1. This figure shows that these data provide a quality sample of various climates. Table 2 gives the station number, location, and number of observations for 1989. Note that station numbers 999** are

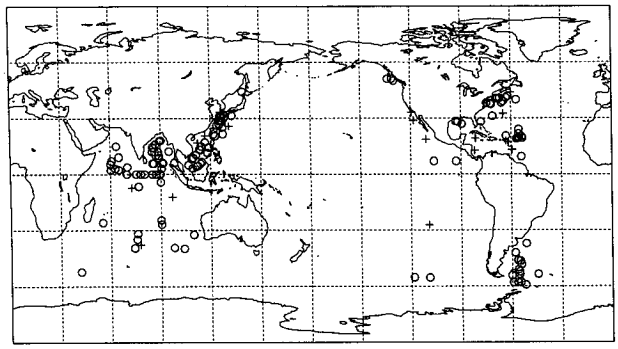

FIG. 1. Locations of the collocated satellite–radiosonde observations for 1989. Circle represents a ship observation and plus indicates a fixed radiosonde station.

ship observations and are shown as circles in Fig. 1. Also note that almost all radiosonde locations are located between 60° and 120°E and 60° and 120°W. Since almost all radiosonde launches were 0000 and 1200 UTC and the SSM/I overpasses were approximately 0600 and 1800 LST, the 2-h temporal coincidence limit effectively removed matches at other longitudes.

Scatter diagrams of radiosonde and satellite CWV for 1989 are presented in Fig. 2. The noticeable differences between these scatter diagrams occur for CWV < 10 kg m^{-2} and CWV > 55 kg m^{-2}. CWV from the SCH and ALI methods for the prior case almost always exceed radiosonde observations, whereas CWV from the PET and GRE methods show less bias. For the latter case, CWV from the ALI method clearly underestimates the radiosonde observations more significantly than the other three retrievals. The presence of outliers occurs in all four comparisons and is consistent for all four satellite retrievals. Since a relative comparison between these retrievals was conducted, outliers were not removed from the data.

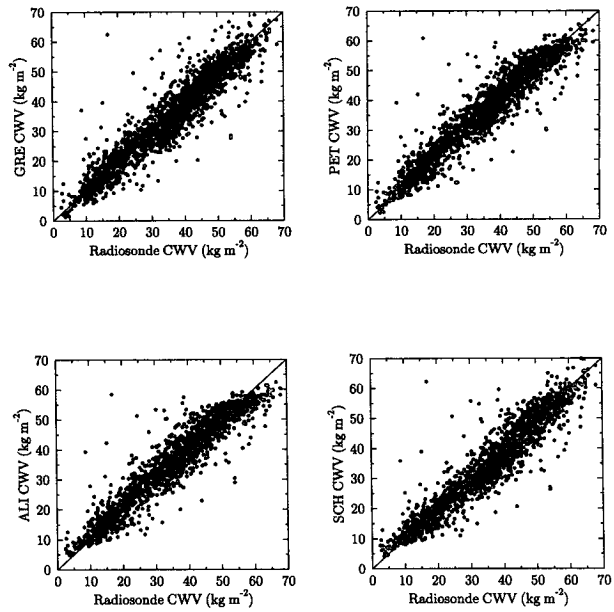

FIG. 2. Scatter diagram of CWV between the satellite retrievals and radiosonde data for 1989.

A more quantitative investigation of the difference between radiosonde and satellite CWV is presented in Table 3. The mean CWV ($\bar{x}$) for both the radiosonde data and satellite retrieved data is highest in JJA and lowest in DJF, whereas the peak standard deviation

TABLE 2. Location and number of observations of the collocated SSM/I observations with the GVaP radiosonde dataset for 1989. Ship observations do not have a particular longitude/latitude.

Station	Latitude	Longitude	Number of Observations
99913	—	—	152
61996	37.80°S	77.50°E	159
85469	27.20°S	109.40°W	63
96996	12.20°S	96.80°E	45
61967	7.30°S	72.50°E	251
99903	—	—	3
99918	—	—	1
80001	12.60°N	81.70°W	105
78954	13.10°N	59.50°W	53
59981	16.90°N	112.30°E	160
78861	17.10°N	61.80°W	41
78866	18.00°N	63.10°W	102
76723	18.70°N	110.90°W	100
78384	19.30°N	81.30°W	147
46810	20.70°N	116.70°E	11
47918	24.30°N	124.20°E	98
47945	25.80°N	131.20°E	43
99912	—	—	3
76151	28.90°N	118.30°W	73
78016	32.40°N	64.70°W	91
72291	33.25°N	119.45°W	40
47185	33.30°N	126.20°E	8
71600	43.90°N	60.00°W	40

TABLE 3. Mean ($\bar{x}$) and standard deviation (σ) for all collocated satellite and radiosonde observations for 1989, and rms difference (R) between satellite and radiosonde observations.

		Radiosonde	Greenwald	Alishouse	Schluessel	Petty
JJA	$\bar{x}$	40.11	40.39	41.01	40.05	41.71
	σ	14.57	14.50	13.64	14.54	14.20
	R	—	5.49	5.16	5.07	5.33
SON	$\bar{x}$	37.04	36.97	37.99	36.86	38.51
	σ	15.61	15.43	14.72	15.23	15.23
	R	—	4.96	4.77	4.75	4.86
DJF	$\bar{x}$	31.79	30.02	31.62	30.01	31.85
	σ	13.99	13.74	13.19	13.33	13.58
	R	—	5.27	4.57	5.07	4.55
MAM	$\bar{x}$	33.89	32.37	33.82	32.03	34.18
	σ	13.37	13.15	12.96	12.96	13.28
	R	—	4.63	4.17	4.58	4.17
TOT	$\bar{x}$	35.55	34.73	35.94	34.52	36.36
	σ	14.67	14.70	14.06	14.50	14.53
	R	—	5.08	4.66	4.87	4.72

(σ) occurs in SON. Here $\bar{x}$ for the GRE and SCH methods most closely match the radiosonde data in JJA, whereas $\bar{x}$ for the ALI and PET methods most closely match the radiosonde data in DJF. This result indicates a seasonal change in the CWV from the radiosonde data that is not found in the satellite retrievals. This difference is clearly evident in scatter diagrams constructed for these two seasons. Figure 3 shows the DJF bias in CWV for the GRE and SCH methods in the CWV range between 25 kg m^{-2} and 50 kg m^{-2}, whereas Fig. 4 shows the JJA bias in the other two retrievals for the same CWV range. The reason for this seasonal bias is not known by the authors.

A frequently used parameter when describing the relationship between radiosonde and satellite observations is the rms difference (R). Typically R is used to describe the magnitude of scatter between radiosonde and satellite data. The equation for the rms difference is

$$R = \left[\frac{\sum_{i}^{N} (xr_i - xs_i)^2}{N} \right]^{0.5}, \qquad (6)$$

where xr is the radiosonde observation, xs is the satellite observation, and N is the total number of observations. The unbiased rms difference used in this study was found using

$$R = \left[\frac{\sum_{i} (xr_i - xs_i - B)^2}{N} \right]^{0.5}, \qquad (7)$$

where B is bias defined

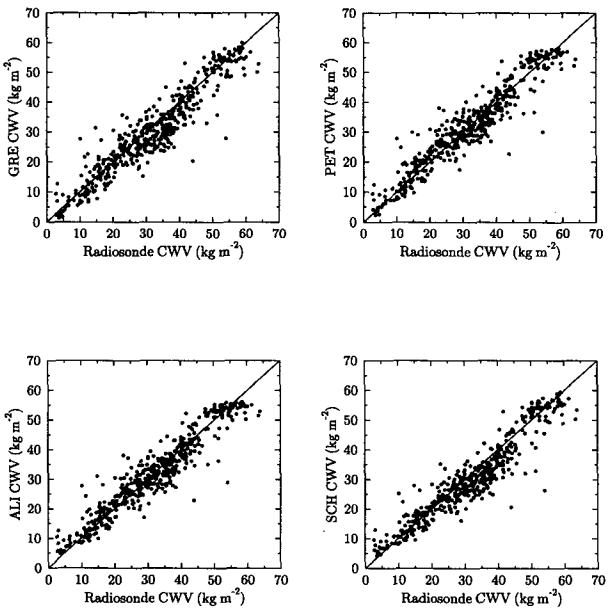

FIG. 3. Same as Fig. 2 except for DJF.

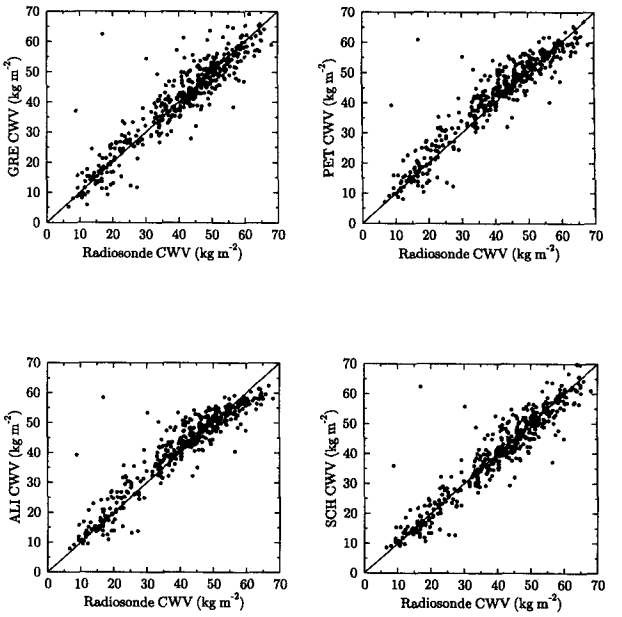

FIG. 4. Same as Fig. 2 except for JJA.

$$B = \frac{\sum_{i} (xr_i - xs_i)}{N}. \qquad (8)$$

These parameters are used in the following discussion to investigate the dependence of R with season along with spatial and temporal sampling.

Table 3 gives the seasonal and annual rms difference for all four satellite retrievals. GRE has the highest annual R of 5.08 kg m^{-2}, whereas ALI has the lowest R of 4.66 kg m^{-2}. These values are generally higher than reported by, for example, ALI since the statistical retrievals are based on the best fit to a select set of radiosonde data and since this study uses different quality controls on precipitation contamination and outliers. The seasonal variation of R changes 1.0 kg m^{-2} from its peak in JJA to the minimum in DJF for the ALI and PET methods, while both the GRE and SCH methods show a second maximum in DJF.

The bias between the satellite retrievals and the radiosonde data can be used to explain where R is effected by systematic bias. Figure 5 shows the bias as a function of CWV over the entire year. All retrievals show positive bias for CWV < 20 kg m^{-2}. The GRE method shows the least amount of bias for this range, whereas the ALI method gives the largest bias. It is for low CWV and high surface wind speeds where the surface roughness of the ocean surface may cause erroneous retrievals of CWV. Most likely the GRE method better accounts for this effect by using an ocean surface roughness model. The notable differences between PET/ALI and GRE/SCH occur for 20 kg m^{-2} < CWV < 50 kg m^{-2}. The bias reverses sign in this range with GRE/SCH estimate less than the radiosonde data. All four retriev-

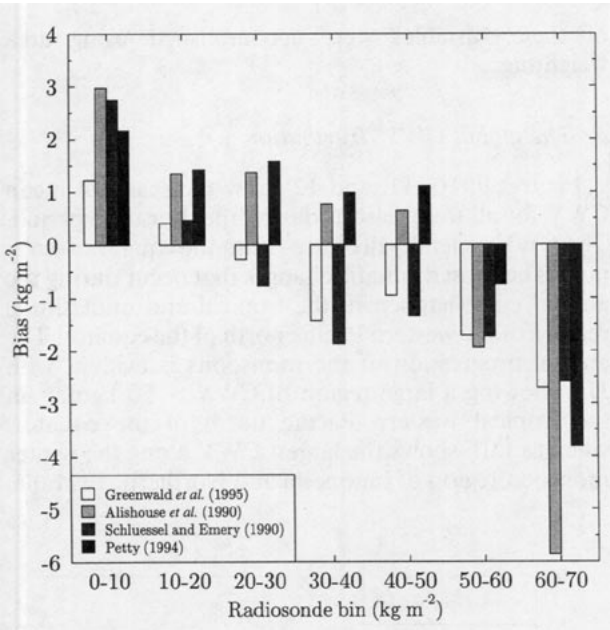

FIG. 5. Bias between the satellite retrievals and radiosonde data for 1989.

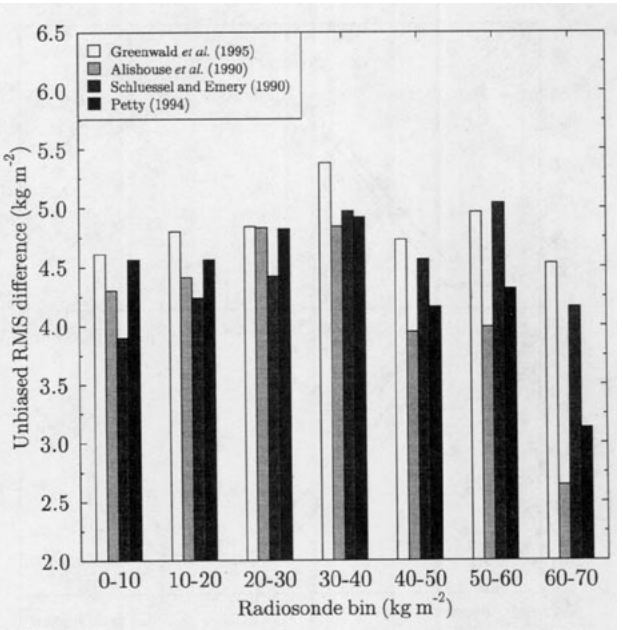

FIG. 6. Unbiased rms difference between the satellite retrievals and radiosonde data for 1989.

als estimate less than the radiosonde CWV for CWV > 50 kg m^{-2} with the ALI method showing the worst bias among the four retrievals.

The unbiased rms difference for each radiosonde CWV bin was examined in order to separate out the effect of a systematic bias on R. Figure 6 shows that the unbiased rms difference is generally greatest for the GRE method. Since statistical retrievals are fitted so that the rms difference is minimized, it was expected that this physical retrieval would have more random scatter. Both the GRE and SCH methods show much greater rms differences for CWV > 60 kg m^{-2} than the PET and ALI methods. These results show that generally the statistical schemes exhibit less overall random error, but are subject to greater bias for low and high CWV. The GRE method generally has more random error and greater bias for the middle range CWV, but less overall bias for low and high CWV values.

Another factor that can effect R is the selection of the time and spatial coincidence between satellite pixels and radiosonde observations. Table 4 shows R between CWV from the GRE method and radiosonde data for various time and spatial constraints. By decreasing the time coincidence from 2 h to 0.5 h, R is reduced nearly 0.6 kg m^{-2}. However, decreasing the spatial coincidence from 50 to 20 km actually *increases* R by about 0.3 kg m^{-2}. This increase is due, in part, to a reduction in the statistical sample size. Spatial coincidence limits greater than 50 km were not investigated, but R is expected to increase for larger spatial limits because the radiosonde observations would be located farther outside of the satellite footprint.

c. *Global satellite-retrieved CWV comparison*

The zonal profiles of the Northern Hemisphere (NH), Southern Hemisphere (SH), and global mean CWV for 1989 as derived from the four different retrieval methods are shown in Fig. 7. The PET method predicted the highest global mean CWV to be 27.17 kg m^{-2} with the ALI, GRE, and SCH methods predicting 27.11, 26.14, and 25.95 kg m^{-2}, respectively. All four retrieval methods showed the same seasonal variability for both hemispheres and over the globe.

Differences between these four retrieval methods were further investigated by examining the zonally averaged CWV. Figure 8a shows the latitudinal distribution of CWV for the GRE method for 1989, whereas Fig. 8b shows the differences between the GRE method and the other three methods. The location of the maximum zonally averaged CWV occurs at 5°N. This maximum is associated with the annually averaged location of the intertropical convergence zone, which is normally identified as region with distinct maxima in precipitation and cloud cover between 0° and 10°N (see Peixoto and Oort 1992). The secondary maximum at 5°S is associated with the high CWV values found in this region during the boreal winter. Generally, the

TABLE 4. Rms difference (kg m^{-2}) between CWV from the GRE method and radiosonde data for different spatial and time constraints.

	20 km	35 km	50 km
2.0 h	5.33	5.17	5.08
0.5 h	4.74	4.45	4.41

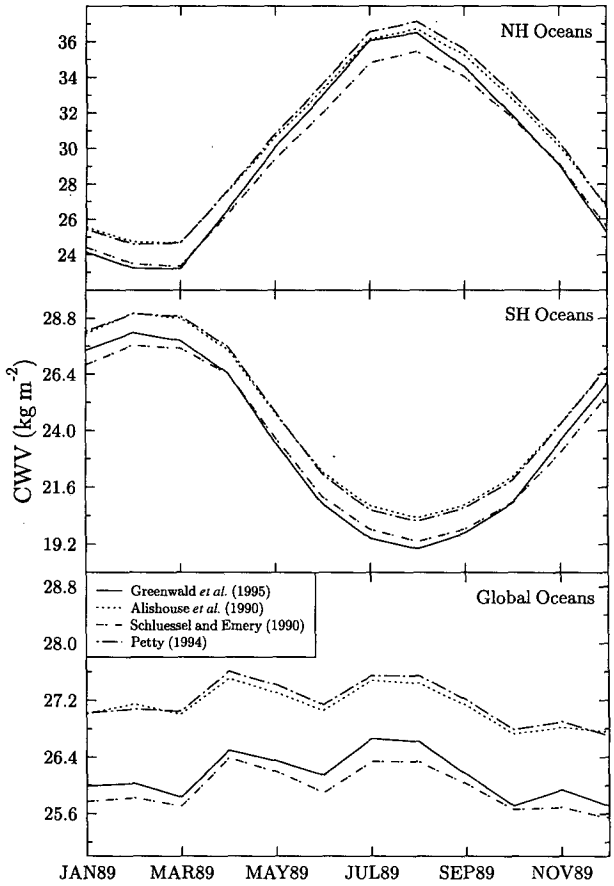

FIG. 7. Time series of the hemispheric and globally averaged oceanic CWV for each satellite retrieval method in 1989.

PET and ALI methods predict more CWV between 30°S and 30°N than the GRE method and this difference accounts for the higher hemispheric and global mean values of CWV for these schemes. All three difference curves exhibit a similar behavior with peaks near 50°N, 50°S, and 5°N. The peak at 5°N is due to the greater underestimation of CWV by statistical schemes for the highest CWV. The GRE method is relatively dry in the subtropics in relation to the PET and ALI methods; however, all the methods retrieve about the same CWV in the midlatitudes. Poleward of 50°N and 50°S, the GRE method once again retrieves less water vapor than the statistical methods, which indicates the larger moist bias the statistical retrievals have in dry climates.

5. CWV climatological results

This section analyzes 4 years (July 1987–June 1991) of CWV derived using the GRE method. Interannual and seasonal variations of CWV are examined over the entire globe. The relationship between CWV and SST is also described. All hemispheric and global averaging of these variables were accomplished using area weighting.

a. The global CWV distribution

Figures 9, 10, 11, and 12 show the seasonal mean CWV for all four seasons during the 4-yr time period. The CWV generally decreases from the equator to each pole. The most dramatic changes that occur during the annual cycle happen in the tropical and midlatitude regions of the western Pacific north of the equator. The annual progression of the monsoons is evident with JJA showing a large region of CWV > 50 kg m^{-2} in the tropical western Pacific north of the equator, whereas DJF shows the largest CWV along the winter monsoon region of Indonesia and Northern Australia.

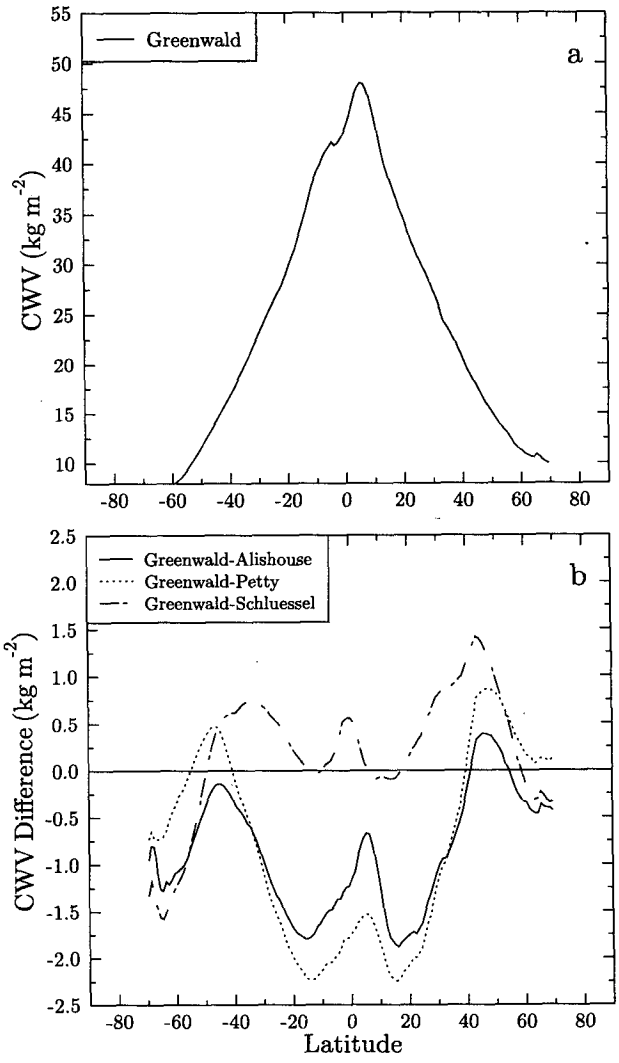

FIG. 8. (a) Zonally averaged CWV from the GRE method for 1989. (b) Difference between CWV from the GRE method and the other three retrievals (Greenwald-statistical) for 1989.

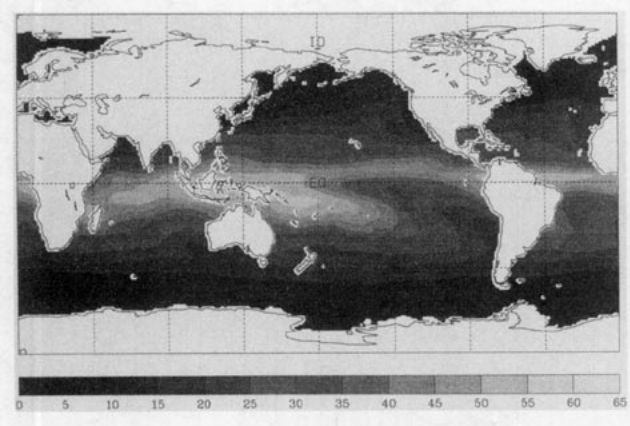

FIG. 9. CWV (kg m^{-2}) for DJF averaged over four years (July 1987–June 1991).

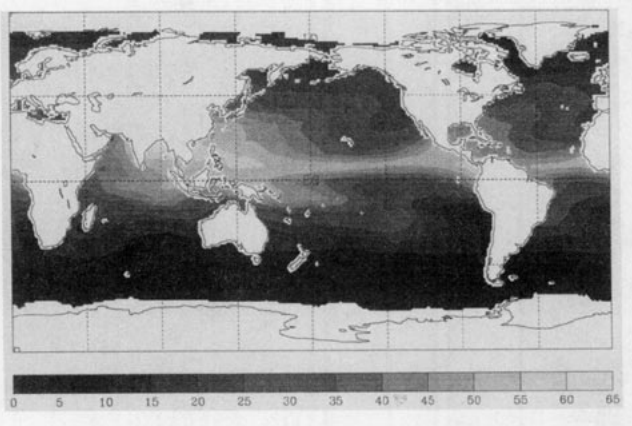

FIG. 11. Same as Fig. 9 except for JJA.

Subtropical high regions off the west coast of South and North America are characterized by CWV values approaching 15 kg m^{-2}. These are regions of persistent subsidence that act to dry the free atmosphere above the boundary layer.

Time series of the total water vapor mass in Fig. 13 shows significant interannual variability in the global oceanic water vapor mass. The total oceanic water vapor mass shows a maximum of 9.77×10^{15} kg in August 1987 and a minimum of 9.15×10^{15} kg in December 1988. The maximum (minimum) coincides very well with the 1986/87 El Niño (1988/89 La Niña), and a 6.5% change in the global oceanic water vapor mass occurred from maximum to minimum. The 4-yr average water vapor mass is 9.33×10^{15} kg. This value is 30% larger than the value reported by Stephens (1990) using SMMR data over the global oceans; however, Stephens (1990) value is erroneously low given his reported annually averaged CWV of 25.8 kg m^{-2}. Assuming roughly 70% global oceanic coverage, the total oceanic water vapor mass from the SMMR results should be 9.2×10^{15} kg, which is only 1.4% less than the GRE total oceanic water vapor mass. Comparisons with water vapor mass data averaged over the entire globe show that the GRE value is 36% smaller than the value calculated by Trenberth et al. (1987) using the European Centre for Medium-Range Weather Forecasts (ECMWF) analysis, and 29% smaller than the value stated in Peixoto and Oort (1992), who used a climatology of radiosonde data.

The hemispheric water vapor mass in Fig. 13 shows a periodic annual cycle. The SH water vapor mass is on average greater than the NH because the SH has a larger oceanic surface area. Over the 4-yr period, the annual variation of water mass in the NH reached its minimum in February and maximum in August, while the SH CWV time series was 180 degrees out of phase with the NH. The NH has an average annual amplitude of 9.2×10^{14} kg (20% change), while the SH has an average annual amplitude of 8.3×10^{14} kg (17% change).

b. The relationship between SST and CWV

The familiar relationship between SST and CWV derived for the 4 years of data is given in Fig. 14. Error

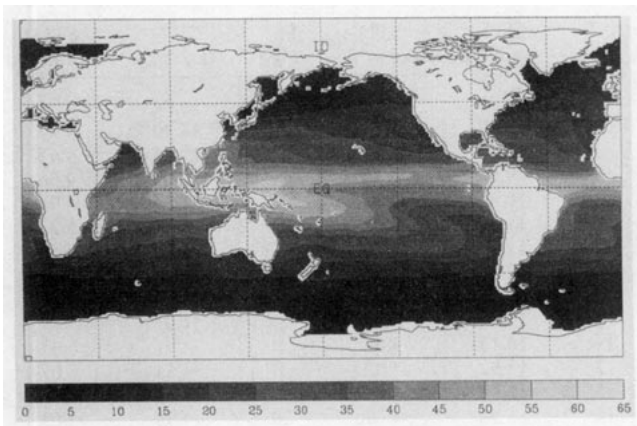

FIG. 10. Same as Fig. 9 except for MAM.

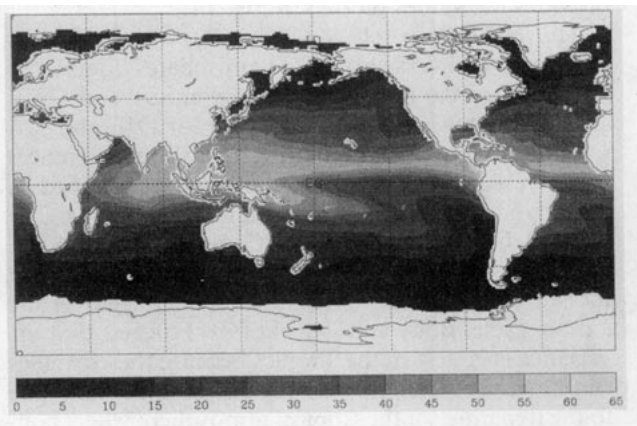

FIG. 12. Same as Fig. 9 except for SON.

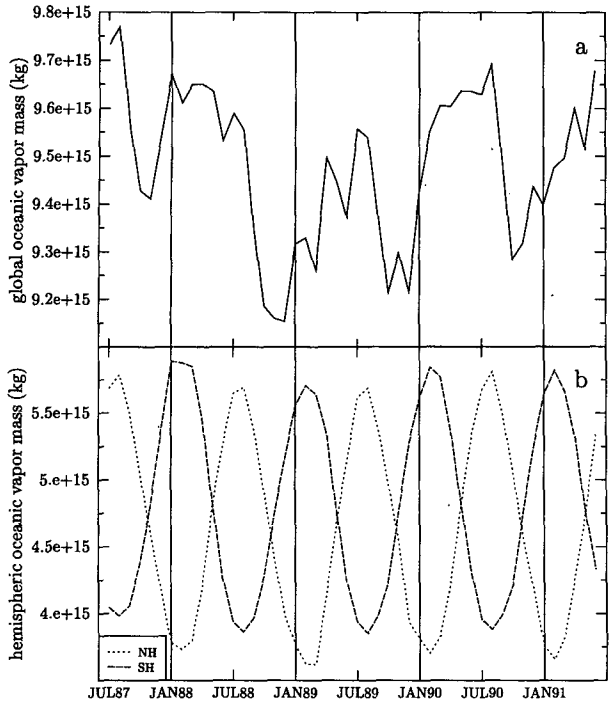

FIG. 13. (a) Time series of global water vapor mass (kg) from July 1987 to June 1991. (b) Time series of Southern Hemisphere (SH) and Northern Hemisphere (NH) total water vapor mass over the ocean.

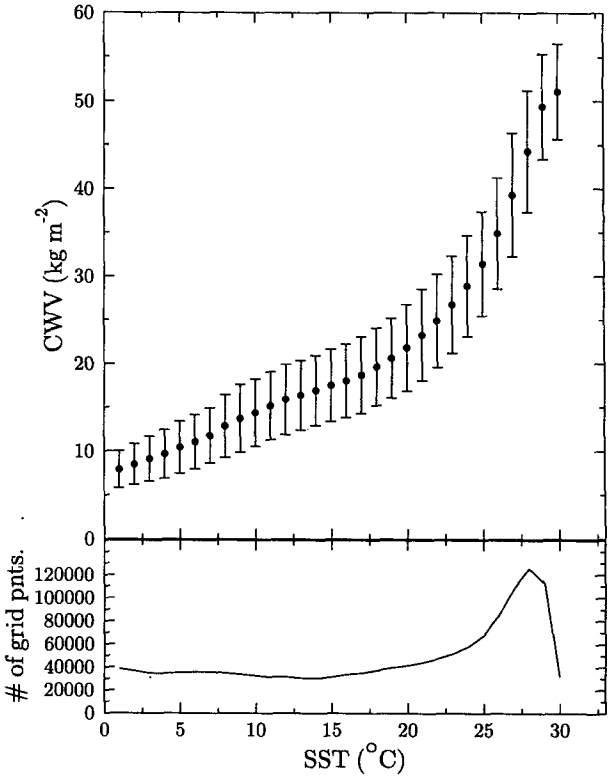

FIG. 14. The mean CWV derived from the GRE method for 1^{circ}C SST bins over the 4-yr period from July 1987–June 1991. Error bars indicate one standard deviation from the CWV mean.

bars indicate one standard deviation from the monthly mean CWV from its 4-yr mean. Deviations were generally less than 5 kg m^{-2} with the largest deviations occurring at the warmest SSTs. These results compare well with the SMMR CWV results described in Stephens (1990) and the CWV derived using the retrieval of Wentz (1983) described in Bony and Duvel (1994). The CWV presented in Stephens (1990) is generally wetter for SSTs > 15°C and drier for colder SSTs, whereas the results presented in Bony and Duvel (1994) are very close to the current data for SSTs < 25°C but significantly wetter over the warmest SSTs. Table 5 provides the values plotted in Fig. 14.

The relationship between SST and CWV was further broken down into season and hemispheres. Figures 15 and 16 show the relationship between SST and CWV separated between the NH and SH for DJF and JJA seasons during the 4-yr period. The striking differences between seasons and hemispheres can be explained by both dynamical and thermodynamic arguments. The tropical differences (SST > 25°C) between season and hemisphere are smaller because the temperature and moisture profiles do not significantly change over the annual cycle. Bony and Duvel (1994) suggest that the variance is largest in the Tropics because these profiles can be vastly different over regions of equal SST due to the dynamics of the tropical atmosphere where convection and subsidence profoundly effect the structure of these profiles. The midlatitude and polar regions (SST < 20°C) show less variance in the CWV for a given SST bin; however, the mean CWV shows a significant difference for different seasons. The winter hemispheric atmosphere in the midlatitudes is generally colder and drier than the summer hemisphere, thus

TABLE 5. SST, CWV, and standard deviation (STD) corresponding to Fig. 14.

SST (°C)	CWV (kg m^{-2})	STD (kg m^{-2})	SST (°C)	CWV (kg m^{-2})	STD (kg m^{-2})
1	7.92	2.12	16	18.04	4.20
2	8.50	2.34	17	18.70	4.40
3	9.13	2.56	18	19.64	4.45
4	9.67	2.77	19	20.65	4.56
5	10.45	2.95	20	21.83	4.96
6	11.06	3.08	21	23.30	5.23
7	11.79	3.13	22	24.90	5.33
8	12.86	3.58	23	26.77	5.56
9	13.72	3.86	24	28.89	5.77
10	14.39	3.85	25	31.43	5.97
11	15.17	3.88	26	34.91	6.37
12	15.92	4.02	27	39.34	7.07
13	16.39	3.97	28	44.33	6.95
14	16.94	4.01	29	49.38	5.99
15	17.51	4.14	30	51.13	5.42

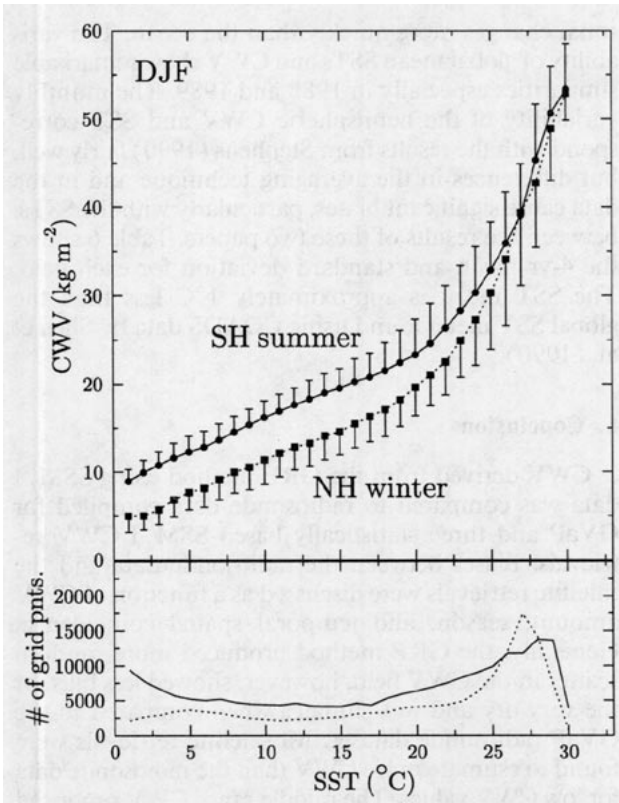

FIG. 15. Same as Fig. 14 except for JJA over the 4-yr period.

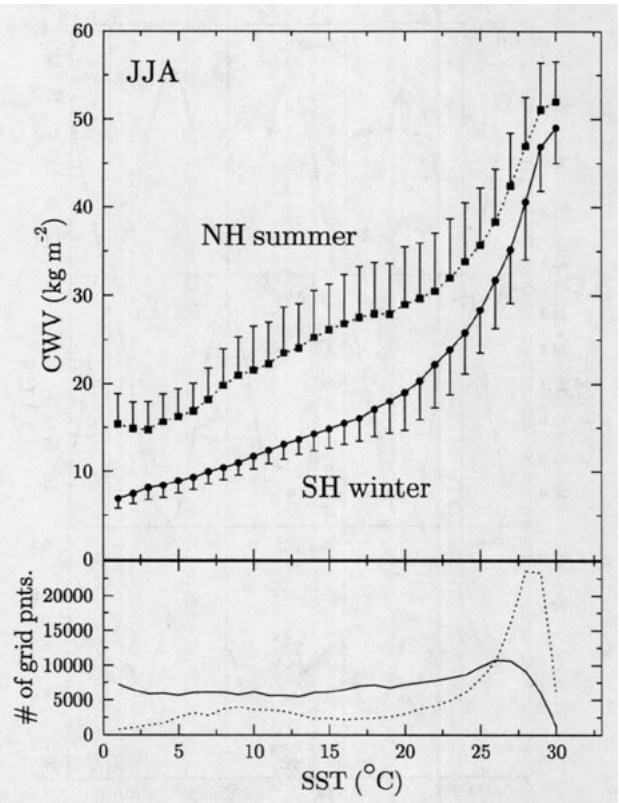

FIG. 16. Same as Fig. 14 except for DJF over the 4-yr period.

the summer CWV values are higher for given SST. The Northern Hemispheric summer is most likely more moist than the Southern Hemispheric summer because northward meridional transport of water vapor over relatively cool SSTs in the western Pacific is large during JJA (Peixoto and Oort 1992).

While these diagrams provide a broad understanding of global, hemispheric, and seasonal relationship between SST and CWV, the global 4-yr correlation of CWV with SST provides further insight into the seasonal and interannual relationship between these quantities. In Stephens (1990), a Clausius–Clapeyron-type relationship between SST and CWV was defined as

$$\mathrm{CWV} = 10.82\left(\frac{r}{1+\gamma}\right)\exp[a(T_s - 288)], \quad (9)$$

where a is a predetermined constant (0.064 K^{-1}), r is the mixing ratio, and γ is the scale height of water vapor. The factor $r/(1+\gamma)$ was found using a least-squares fitting of the current data. Figure 17 shows the monthly mean 4-yr correlation between the observed SST and the SST predicted by (9) given the retrieved CWV. The highest correlations ($r > 0.9$) occur in the central northern Atlantic and Pacific (25°–50°N) and in smaller regions in the southern central Pacific and Indian oceans (25°–35°S). Weaker correlation (0.6–0.8) was found south of 60°S, north of 60°N in the storm-track regions, and in tropical regions where deep convection is less persistent. No significant correlation between SST and CWV is found in the Indonesia region, along the Somali Current off the coast of eastern Africa, off the eastern coast of South America near the mouth of the Amazon, or west of Panama.

Regions where r exceeds 0.9 indicate areas of large-scale subsidence associated with persistent subtropical

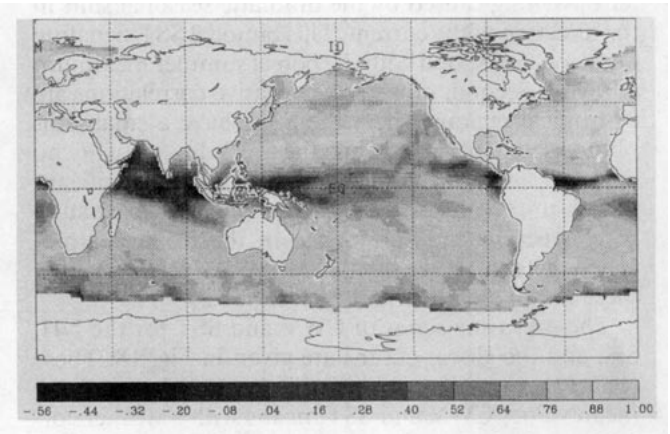

FIG. 17. Global map of the linear correlation between observed SST and SST derived from (9) using the CWV from the GRE method over the 4-yr period from July 1987 to June 1991.

——, H. M. Woolf, C. M. Hayden, D. Q. Wark, and L. M. McMillin, 1979: The *TIROS-N* Operational Vertical Sounder. *Bull. Amer. Meteor. Soc.*, **58,** 1177–1187.

Starr, D. O'C., and S. H. Melfi, 1991: The role of water vapor in climate: A stategic research plan for the proposed GEWEX water vapor project (GVaP). NASA Conf. Publ. 3120, National Aeronautics and Space Administration, Washington, D.C., 50 pp.

Starr, V. P., J. P. Peixoto, and R. G. McKean, 1969: Pole-to-pole moisture conditions for the IGY. *Pure Appl. Geophys.*, **75,** 300–331.

Stephens, G. L., 1990: On the relationship between water vapor over the oceans and sea surface temperature. *J. Climate,* **3,** 634–645.

——, D. L. Jackson, and J. J. Bates, 1994: A comparison of SSM/I and TOVS column water vapor data over the global oceans. *Meteor. Atmos. Phys.*, **54,** 183–201.

Tjemkes, S. A., G. L. Stephens, and D. L. Jackson, 1991: Spaceborne observation of columnar water vapor: SSMI observations and algorithm. *J. Geophys. Res.*, **96,** 10 941–10 954.

Trenberth, K. E., J. R. Christy, and J. G. Olson, 1987: Global atmospheric mass, surface pressure, and water vapor variations. *J. Geophys. Res.*, **92,** 14 815–14 826.

Wentz, F. J., 1983: A model function for ocean microwave brightness temperatures. *J. Geophys. Res.*, **88,** 1892–1908.

——, 1992: User's manual SSM/I antenna temperature tapes. Rev. 1. Remote Sensing Systems Tech. Rep. 120191. [Available from Remote Sensing Systems, Inc., Santa Rosa, CA 95404.]